ACADEMIC PRESS

Available online at www.sciencedirect.com
SCIENCE DIRECT®

Journal of Catalysis 217 (2003) 376–387

JOURNAL OF CATALYSIS

www.elsevier.com/locate/jcat

New insights into parameters controlling the selectivity in hydrocracking reactions

E. Benazzi,[a] L. Leite,[a,1] N. Marchal-George,[b] H. Toulhoat,[c] and P. Raybaud [d,*]

[a] *Division Cinétique et Catalyse, Institut Français du Pétrole, 1 & 4 avenue de Bois-Preau, 92852 Rueil-Malmaison cedex, France*
[b] *Division Développement, Institut Français du Pétrole, 1 & 4 avenue de Bois-Preau, 92852 Rueil-Malmaison cedex, France*
[c] *Direction Scientifique, Institut Français du Pétrole, 1 & 4 avenue de Bois-Preau, 92852 Rueil-Malmaison cedex, France*
[d] *Division Chimie et Physico-Chimie Appliquées, Institut Français du Pétrole, 1 & 4 avenue de Bois-Preau, 92852 Rueil-Malmaison cedex, France*

Received 5 November 2002; revised 21 January 2003; accepted 21 January 2003

Abstract

Improving the selectivity of the transformation of heavy oils into valuable middle distillates represents one of the current challenges for hydrocracking (HCK) catalysts. For that purpose, new insights are required for a better design of HCK catalysts. We choose the hydrocracking of phenanthrene as a model reaction in order to compare several mesoporous and microporous acid solids. Characterization of the acidity of the solids reveals that there is no direct correlation between the HCK selectivity and the solids acidity. Moreover, combining the results of catalytic tests and force-field simulations, we are able to show that diffusional limitations can be ruled out and that the key phenomenon adversely affecting the selectivity is a too strong adsorption of isomerized products which favors overcracking. Below a steric exclusion threshold, pore size controls energies by virtue of confinement effects. Optimal solid acid HCK catalysts should therefore be designed by taking those effects into account.

Keywords: Hydrocracking; Bifunctional catalyst; Zeolite; Silica-alumina; Phenanthrene; Selectivity; Force-field simulation; Adsorption energy

1. Introduction

In the past 10 years, the growing demand for middle distillates [1] combined with more stringent specifications concerning diesel cuts, in order to minimize the environmental impact of automotive fuels, has increased the importance of the hydrotreating and hydrocracking processes in modern refinery schemes. Thus, there is no doubt that hydrocracking processes will play a key role in producing high-quality diesel fuels that will match future specifications.

High-pressure hydrocracking is a catalytic petroleum refining process that is applied to upgrade the heavier fractions, for instance, vacuum gas-oil obtained from the distillation of crude oils, into high-quality middle distillates (kerosene, gas-oil). Hydrocracking plays a key role in petroleum refining since it is also used to upgrade some of the products obtained from other processes, such as coker gas oil, deasphalted oil, and fluid catalytic cracking (FCC) cycle oils. It is a process of considerable flexibility allowing the conversion of a wide range of feedstocks to a variety of products. The products obtained are of high-quality. Nowadays the European demand for high-quality middle distillates (low sulfur and aromatics contents and high cetane number) is high and one important goal for the refining industry is to selectively transform heavy oils into middle distillates.

Consequently it is of great interest to develop new hydrocracking catalysts that can maximize the formation of high-quality middle distillates. Hydrocracking occurs via a bifunctional scheme [2,3] and commonly involves catalysts presenting acidic and hydrogenating functions. Schematically typical acidic supports used are amorphous silica-alumina, zeolites, and more especially Y and USY zeolites and fluorine-doped alumina [4,5], whereas the hydrogenating function consists of NiMo, CoMo, or NiW sulfides and in some cases of noble metals.

Y zeolite-based catalysts are more active than amorphous-based catalysts [6] and can operate at lower reaction temperatures, which favors the hydrogenation of the aromatics

* Corresponding author.
E-mail address: pascal.raybaud@ifp.fr (P. Raybaud).
[1] Current address: Rhodia, 52 rue de la Haie Coq, 93308 Aubervilliers, France.

0021-9517/03/$ – see front matter
doi:10.1016/S0021-9517(03)00041-1

present in the feed and increases the cetane number of the produced diesel. Nevertheless, Y zeolite-based catalysts are less selective to middle distillates than amorphous-based catalysts [7]. Therefore, in order to maximize the production of high-quality middle distillates it would be highly interesting to design hydrocracking catalysts combining the good activity of the zeolite-based catalysts and the selectivity of the amorphous silica-alumina.

In order to design better hydrocracking catalysts, knowledge of the transformation of the different kinds of molecules present in the industrial feedstocks and understanding of the phenomenon involved in the different type of catalysts are necessary.

Numerous studies have been devoted to the hydrocracking of model compounds like paraffins (n-C_6 to n-C_{10}) and this is now well understood [8,9]. However, these molecules do not fully represent heavy petroleum fractions and detailed studies on hydrocracking of larger molecules with more than 10 carbon atoms are rather rare in the literature [10–12].

Recently, we developed a new hydrocracking model reaction using a bulky molecule, the phenanthrene (with 3D characteristic dimensions $x = 11.1$ Å, $y = 7.5$ Å, and $z = 3.4$ Å), allowing a better description and understanding of phenomena involved in the hydrocracking processes [13]. In our previous works, we studied the hydrocracking of phenanthrene over platinum on various acidic supports (silica-alumina and zeolites) and we showed that the first step in its transformation is a total hydrogenation reaction which leads to perhydrophenanthrene, a bulky naphtenic C_{14} compound (with 3D dimensions such as $x = 11.4$ Å, $y = 6.9$ Å, and $z = 5.1$ Å) [14].

In the present work, we studied the catalytic performances of Pt catalysts based on various acidic phases (H-MFI, H-Beta, H-USY zeolites, amorphous silica-alumina, and MCM-41), presenting different pore apertures, porosities, topologies, and acidities, for the hydrocracking of phenantrene at 6.0 MPa. The influence of the acid site density and strength has also been studied in the case of the H-Y, H-β zeolites, and amorphous silica-aluminas. Our final objective is to compare these hydrocracking catalysts in term of activity and selectivity with respect to our model reaction and to correlate the catalytic performances with solid properties.

2. Methods

2.1. Experiments

2.1.1. Model reaction

Phenanthrene used in the present study was obtained commercially and used without further purification. Hydrocracking reactions were performed in a fixed-bed continuous flow reactor equipped with liquid and gas collectors. In order to be pumped, phenanthrene was dissolved in cyclohexane in the concentration of 4 wt%. Experiments were performed under 60 bar total pressure (H_2 partial pressure of 51 bar) and with a molar ratio H_2/Hydrocarbon of 6. Reactions were carried out at 573 and 603 K. Under these conditions, all catalysts are stable and the solvent transformation is limited to isomerization into methylcylopentane [13]. The conversion of phenanthrene was varied by modifying the contact time t_c between catalyst and hydrocarbon (t_c = feed flow/catalyst volume). Both liquid and gas products were analyzed quantitatively by a gas chromatograph (Hewlett Packard 5890) equipped with a 50-m-length PONA column. The column temperature was controlled at 313 K for 10 min and then heated to 553 K at a heating rate of 2 K/min. Identification of the products formed during phenanthrene hydrocracking was performed by GC-MS analysis.

2.1.2. Catalysts

The 11 acid solids studied were 3 silica-alumina samples with different silica contents, 30, 40, and 90 wt% obtained from Condea, a MCM-41 mesoporous solid prepared according to [15], 4 Y zeolite samples with Si/Al varying from 5.7 to 73, and a ZSM-5 sample obtained from Zeolyst. Finally, two β zeolite samples were used: the first one, with Si/Al = 10.5, was furnished by Zeolyst, and the second one was obtained by dealumination of the previous β sample according to [16]. The zeolitic bifunctional catalysts were obtained by shaping the zeolites described above with alumina and by depositing Pt on the obtained supports by cationic exchange with NH_4NO_3 as competitor and $Pt(NH_3)_4Cl_2$ as platinum precursor.

The physico-chemical characteristics of these solids are described in Tables 1, 2, and 3 and the composition of these catalysts is summarised in Table 4.

The acidity of the studied solids (Table 3) was probed by 2,6-dimethylpyridine (lutidine), according to a similar method as described in Refs. [17,18]. Samples of 20 mg were pressed into disks and introduced in the IR cell and then activated in situ by heating under dynamic vacuum (10^{-6} Torr) at 573 K for 18 h. After cooling to 423 K, lutidine was adsorbed and the spectra were recorded after 2 h desorption at this temperature under dynamic vacuum. In the study of the desorption of lutidine at 573 K, the spectra were recorded after only 1 h of desorption under dynamic vacuum. The spectra were recorded with a Nicolet FTS-40 FTIR spectrometer.

Pt content in each catalyst was determined using X-ray fluorescence analysis. The metal dispersions were measured by H_2 chemisorption and H_2–O_2 titration. Because of their strong acidity compared to amorphous silica-alumina, H-Y, and H-β zeolites were diluted with inert alumina whereas silica-alumina was used pure. Before the experiments, catalysts were calcined in a stream of air at 693 K for 4 h and then reduced under H_2 flow at 723 K for 2 h. As a reference which does not possess bifunctionality, a Pt (0.5 wt%) supported on Al_2O_3 catalyst was prepared.

Table 1
Physico-chemical properties of the microporous solids (zeolites)

Acidic solids	Bulk Si/Al atomic ratio	Framework[a] Si/Al^{IV}	Unit cell size (Å)	Crystallinity (%)	Crystallite size (nm)	Pore opening (Å)	BET (m^2/g)	Pore volume (cm^3/g)		
								Total	Micro[b]	Meso[c]
Y1 (HSZ350HUA)[d]	5.7	6.6	24.43	100	100	7.4	883	0.43	0.34	0.09
Y2 (CBV720)[e]	17.7	23	24.29	83	1000	7.4	892	0.43	0.32	0.11
Y3 (CBV780)[e]	38	–	24.22	71	id.	7.4	854	0.48	0.32	0.16
Y4 (CBV790)[e]	73	–	24.15	44	id.	7.4	793	0.47	0.28	0.19
$\beta 1$ (CP811E.1)[e]	10.5	–	–	100	15–50	6.4×7.6	636	0.25	0.25	0
$\beta 2$[f]	94	–	–	100	id.	6.4×7.6	733	0.25	0.25	0
ZSM-5 (CBV8020)[e]	37.3	–	–	–	300–1000	5.3×5.6	410	–	–	0

[a] Calculated by the Fichtner–Schmittler correlation.
[b] Microporous volume obtained by the *t*-plot method.
[c] Mesoporous volume calculated $V_{meso} = V_{tot} - V_{micro}$.
[d] Sample supplied by Tosoh.
[e] Samples supplied by Zeolyst.
[f] Obtained by acid leaching of sample $\beta 1$ according to the method described in [16].

Table 2
Physico-chemical properties of the mesoporous solids (silica-alumina and MCM-41)

Acidic solids	SiO_2 (wt%)	Al_2O_3 (wt%)	Pore diameter[a] (Å)	BET (m^2/g)	Pore volume[b] (cm^3/g)
Silica-alumina 1 (Condea)	30	70	70–80	343	0.61
Silica-alumina 2 (Condea)	40	60	70–80	300	0.59
Silica-alumina 3	90	10	50	370	0.53
MCM-41[c]	87	13	30	657	1.55

[a] Pore diameter range determined by Hg porosimetry and N_2 adsorption isotherm (BJH method).
[b] From N_2 adsorption.
[c] Prepared according to [15].

Table 3
Brønsted acidity of the acidic solids (arbitrary unit a.u.) as determined by IR spectroscopy with adsorption–desorption of lutidine according to methods described in [17,18]

Samples	Brønsted (a.u.)	
	423 K	573 K
H-Y1	25	17.7
H-Y2	9.8	5.7
H-Y3	2.0	1.4
H-Y4	0.6	0.3
H-$\beta 1$	14.5	11.5
H-$\beta 2$	9.9	8.8
Silica-alumina-1	2.0	0.3
Silica-alumina-2	3.7	0.6
Silica-alumina-3	2.3	0.4
MCM-41	2.7	0.4

Table 4
Characteristics of the studied bifunctional catalysts

Catalysts	Solid acid content in extrudate (wt%)	Pt content in the catalyst (wt%)	Pt content in the zeolite (wt%)	Pt dispersion (%)
Pt/H-Y1	2.5	0.18	7.1	60
Pt/H-Y2	2.5	0.10	4.5	56
Pt/H-Y3	5	0.17	3.3	85
Pt/H-Y4	5	0.17	3.4	83
Pt/H-$\beta 1$	0.5	0.05	10	41
Pt/H-$\beta 2$	2.5	0.16	6.6	53
Pt/H-ZSM-5	5	0.15	3	65
Pt/silica-alumina-1	100	0.60	–	43
Pt/silica-alumina-2	100	0.67	–	60
Pt/silica-alumina-3	100	0.91	–	55
Pt/MCM-41	20	0.67	–	72

2.2. Molecular simulation

For the simulation, we used two main approaches: On the one hand, we used the Sorption module to calculate adsorption enthalpies and loadings at 573 K and 100 kPa for the different relevant reactants and products in FAU, BEA, and VFI ideal siliceous framework. VFI was chosen to mimic the larger pore structure (see next section). On the other hand, we used the Diffusion_Path module to establish energy profiles of aromatic compounds along the diffusion path inside the BEA, FAU, and MFI channels. Sorption and Diffusion_Path are accessible through the Cerius^2 (release 4.0) and InsightII (release 4.0.0P+) interfaces licensed by Accelrys Inc. [19].

2.2.1. Force field

We treat the molecule-zeolite interaction at an atomic level assuming that we can neglect the precise electron distribution for focusing on the main environmental effect due to the different porous properties. For that purpose, we used the Universal Force Field (UFF release 1.02) as implemented in Cerius^2 and InsightII according to Rape et

al. [19,20]. The potential energy of a molecule in the pores depends on its atomic coordinates and can be expressed as the sum of valence-bond terms and nonbond interaction terms. UFF is a purely diagonal and harmonic force field. The van der Waals forces are described by a Lennard–Jones interaction.

For the simulation of hydrocarbon adsorption, the zeolite framework is represented by a repeated unit cell with three-dimensional periodic boundary conditions. The van der Waals interactions are considered only in a sphere within a finite radius, called the cutoff radius using the long-range tail correction [21]. We verified the cutoff convergence with respect to the energy for each zeolite.

2.2.2. Adsorption enthalpy calculations

We used the Grand Canonical Monte Carlo technique to investigate the adsorption configuration of aromatics inside the pores, and to estimate the adsorption enthalpies for a given temperature ($T = 573$ K) and pressure ($P = 100$ kPa), consistent with the conditions of our catalytic experiments. At high temperatures, hydrocarbon molecules are distributed over several sites within the zeolite framework; the "location" becomes a probability distribution and energy an integral over all accessible sites. In the canonical ensemble (μVT), the Metropolis algorithm proceeds by selecting, displacing, inserting and deleting randomly a molecule. The Metropolis scheme generates a Markov chain of states which sample the equilibrium states of the system according to the Boltzmann probability distribution. The equilibrium is achieved when T and μ of the compounds inside the zeolite are equal to those of the free molecule in the gas phase. Depending on the system and on the hydrocarbon, the number of search iterations varies between 10^6 and 5×10^6 before reaching the convergence criterion on the energy (0.05 kcal/mol). The atoms of the zeolite framework are kept fixed and the molecules are supposed rigid. This assumption is completely valid for the phenanthrene molecule. For the other molecules (methylcyclopentanodecaline and methylcyclohexane), we checked our results by sampling the configurations of the adsorbed molecules with molecular dynamics in the gas phase.

2.2.3. Diffusion path simulations

We determine the energy profiles along the diffusion path of relevant C_{14} compounds inside FAU, BEA, and VFI frameworks. The diffusion path calculation is carried out on zeolite supercells duplicating the unit cell along the diffusion axis so as to provide a sufficient length in order to sample at least four periods of the energy profile [22]. The initial pathway is assumed to be a straight line following the channel symmetry axis and connecting two positions located at the center of the pore. The hydrocarbon is forced to move along this pathway by steps of $dx = 0.01$ Å. At each step, the geometry of the hydrocarbon is optimized, allowing atomic displacements in a plane perpendicular to the initial pathway, while the zeolite framework is relaxed. This calculation provides an energy profile along the diffusion pathway. This profile is used to estimate diffusion barriers, under the approximation that entropic contributions to the free energy profile are negligible.

3. Results

3.1. Hydrogenation reaction

A preliminary study using the monofunctional catalyst Pt/Al_2O_3 showed the hydrogenation of phenanthrene to be fast and to achieve completion. In a large range of contact times ($0.1 < t_c(h) < 2$), 100% of phenanthrene is converted into perhydrophenanthrene. No partially hydrogenated phenanthrene species such as dihydro-, tetrahydro-, and octahydrophenanthrene were observed. Under these conditions, platinum can be considered as a very strong hydrogenating agent. This preliminary experiment indicates that in studies with Pt-bifunctional catalysts, we have to consider perhydrophenanthrene molecules as the reactant. Consequently, conversion has been calculated from the disappearance of the six conformational isomers of perhydrophenanthrene [23]. Furthermore, no cracking products were observed for this monofunctional catalyst, allowing us to affirm that thermal cracking does not occur in the reaction temperature range. Finally, with this good hydrogenating function in relatively large quantities, the catalysts present a good metal/acid balance as described by Alvarez et al. [24]. In this situation, the quantity of the hydrogenation component is large enough for the reaction to depend only on the acidic component of the support. This point has been checked in a previous work by studying catalysts with different quantities of platinum [25].

3.2. Hydrocracking reaction

The model reaction was first studied with the silica-alumina-based catalysts. Hydrocracking of phenanthrene on Pt/silica-alumina 1 (Tables 2–4) leads to more than one hundred products detected by gas chromatography analysis (Fig. 1). Ensuing GC-MS analysis allows the classification of these products into three main families. The first one consists of molecules resulting from total hydrogenation of phenanthrene, globally denoted as the perhydrophenanthrene molecules (Fig. 2a). This group is called *C14hydro* and is considered as the reactant group. The second family contains molecules still having 14 carbon atoms but presenting a mass spectrum showing the presence of one or two methylcyclopentyl saturated rings (Fig. 2b). We called these compounds the *C14isom* group. Finally, the last family contains molecules having less than 14 carbon atoms and resulting from a primary (methylcyclohexane, for example) or a secondary (propane or butane) cracking of species with 14 carbon atoms: $C14^-$. Another family of products, the

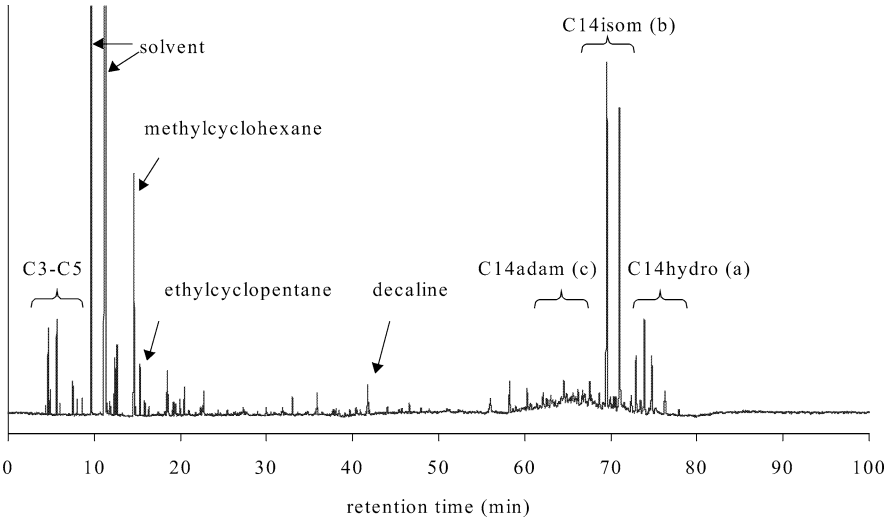

Fig. 1. Chromatogram of liquid products of phenanthrene hydrocracking in the case of catalysts containing Y zeolite or silica-alumina.

alkyl-adamantanes (*C14adam)*, have been identified in liquid products (Fig. 2c). The formation of these molecules during hydrocracking reactions is probably due to a series of carbocationic rearrangements. According to Schneider et al. [26], perhydroaromatics having three rings and 12 or more carbon atoms, undergo rearrangement to form various types of derivatives in the presence of an aluminum halide catalyst. The main products are hydrocarbons of the thermodynamically favored adamantane structure. However, because of their lower concentrations, this parallel reaction will not be especially considered and the *C14adam* group will be brought together with the *C14isom* products in order to form a group of products having 14 carbon atoms products and called *C14prod.* This group does not include the *C14hydro* products which are considered as the reactants.

The evolution with contact time of products yields at 573 K for the silica-alumina-based catalyst is represented in Fig. 3. At this stage, it must be emphasized that similar trends are observed for the catalysts containing silica-aluminas, MCM-41, or H-Y zeolites. For these catalysts, we propose the apparent reaction pathway described in Fig. 4. Isomerization products are primary products whereas cracked products appear to be secondary products. Cracked products are essentially 7 carbon atoms products such as methylcyclohexane, dimethylcyclopentane, or ethylcyclopentane which can be also submitted to further cracking to give lighter products (mainly propane and butane) depending on the operating conditions (reaction temperature and contact time) and the catalyst type. It seems that the central ring is preferentially cracked. We have previously proposed a mechanism in order to explain the obtained products distribution [13]. No cracked products with 10 carbon atoms were observed, which differs from the study of Haynes et al. [27]. In their work, hydrogenation of phenanthrene was not achieved, so perhydrophenanthrene molecules were replaced by partially hydrogenated phenanthrene. Thus, the cracking of these molecules occurs in a different manner.

In the case of catalysts containing H-Beta zeolite, the analysis of the reaction products has shown that bicyclohexyl-type compounds (such as ethylbicyclohexyl) and alkylnaphtyl-type compounds were also formed. They are probably obtained from the transformation of the perhydrophenanthrene molecules via isomerization and ring opening reactions. The bicyclohexyl and alkylnaphtyl-type compounds possess 14 carbon atoms like perhydrophenanthrene products but present a higher molecular weight, 194 g/mol (determined by mass spectrometry), compared to 192 g/mol for the perhydrophenanthrene. The bicyclohexyl and alkylnaphtyl-type compounds can be cracked after isomerization reactions in order to lead to cracked products which are the same as those observed with the other catalysts.

Consequently, in order to take into account the particular behavior of the H-Beta zeolite catalysts, we defined the group of products having 14 carbon atoms as *C14prod*, including the *C14isom* products, the *C14adam*, the bicyclohexyl, and the alkylnaphtyl-type compounds. As in the case of H-Y, MCM-41 and silicas-aluminas, the *C14prod* group excludes the *C14hydro* products considered as reactants. The second group, $C14^-$, contains molecules having less than 14 carbon atoms and resulting from a primary (methylcyclohexane, for example) or a secondary (propane or butane) cracking of species with 14 carbon atoms. With these definitions of $C14^-$ and *C14prod*, similar trends as in Fig. 4, are observed for H-Beta catalysts.

In what follows, we compare the catalytic performances on the basis of the selectivity in cracked products ($C14^-$) and products having 14 carbon atoms (*C14prod*) defined as the yield in cracking or *C14prod* at a given conversion of 60 wt% (unless specified otherwise).

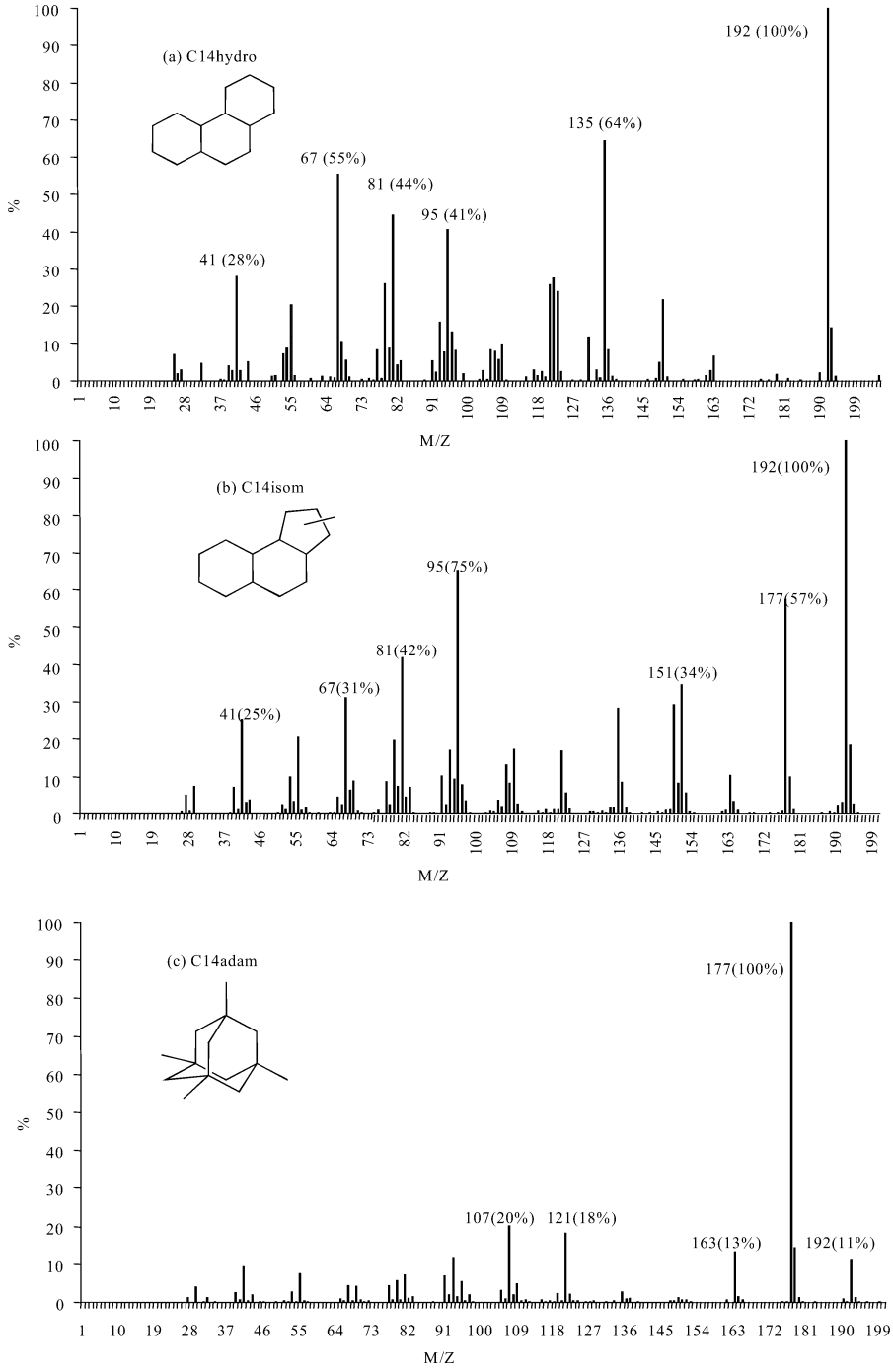

Fig. 2. Mass spectra of *C14hydro* (a), *C14isom* (b), and *C14 adam* (c) products.

3.3. Effect of temperature on the reaction

Fig. 5 shows the yield in *C14isom* products versus conversion for the silica-alumina-based catalyst for two temperatures: 573 and 603 K. Again, similar results are observed for the other catalysts tested within our work. It can be clearly seen that a temperature increase has a strong effect on yields. At 603 K, cracking reactions are favored to the detriment of isomerization reactions. For example, at a conversion level of 75%, *C14isom* yield is 48% at 573 K and 36% at 603 K. These results indicate that the comparison of catalytic performances between different solids acid needs to be performed at the same temperature (a reaction temperature of 573 K was chosen for the what follows). If it is not rigorously the case, the temperature effect could hide the effect of solid properties. The apparent activation energy for all catalysts was calculated to be between 25 and 30 kcal/mol, in agreement with literature values for hydroconversion of naphtenic feeds over Pt/solid acid-based catalysts [28].

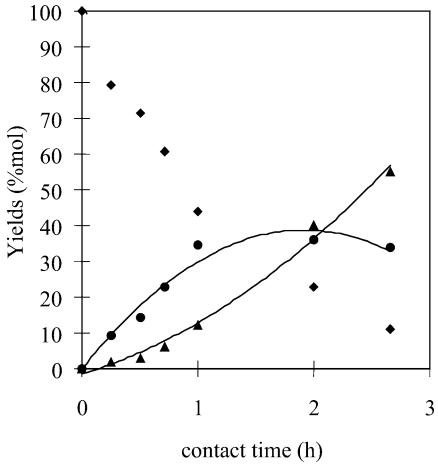

Fig. 3. Reaction product yields: *C14hydro* (◆), *C14isom* (●), and $C14^-$ (▲), as a function of contact time ($T = 573$ K, pressure = 6 MPa) over Pt/silica-alumina-1.

3.4. Effect of acidity

In this work, the calculated activity is the number of moles of perhydrophenanthrene converted per hour and per gram of solid acid. That is to say that we have taken into account the zeolite content of the catalysts. In the case of silica-alumina catalysts, the support totally contains silica-alumina and consequently no dilution factor is considered. We demonstrate here clearly that H-Y zeolite and H-β zeolite (i.e., large pore zeolite)-based catalysts are effective in processing bulky molecules having dimensions of the same order as phenanthrene.

Experimentally, differences in activity were observed during the hydrocracking of phenanthrene over the 10 Pt/acidic solids studied in this work. The Pt/silica-aluminas, Pt/MCM-41, and the Pt/highly dealuminated Y zeolite exhibit lower catalytic activities as illustrated by Fig. 6, where it appears that the catalytic activity is correlated to the number of Brønsted acid sites in the acidic solids determined by infrared spectroscopy with adsorption–desorption of lutidine (see also Table 3).

It can be assumed that the activity differences observed among zeolites and between silica-aluminas and zeolites

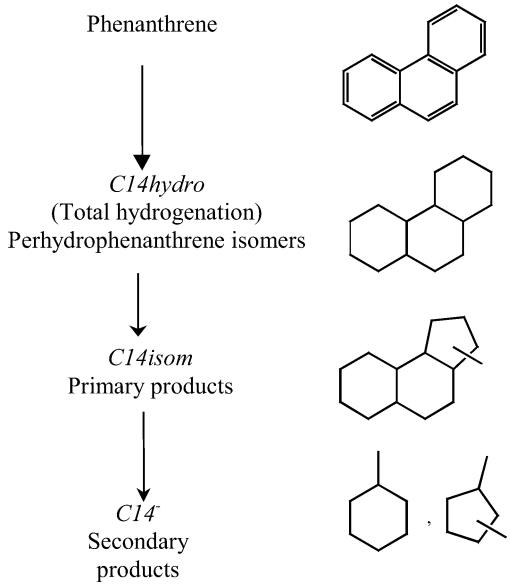

Fig. 4. Proposed reaction pathway for phenanthrene hydrocracking.

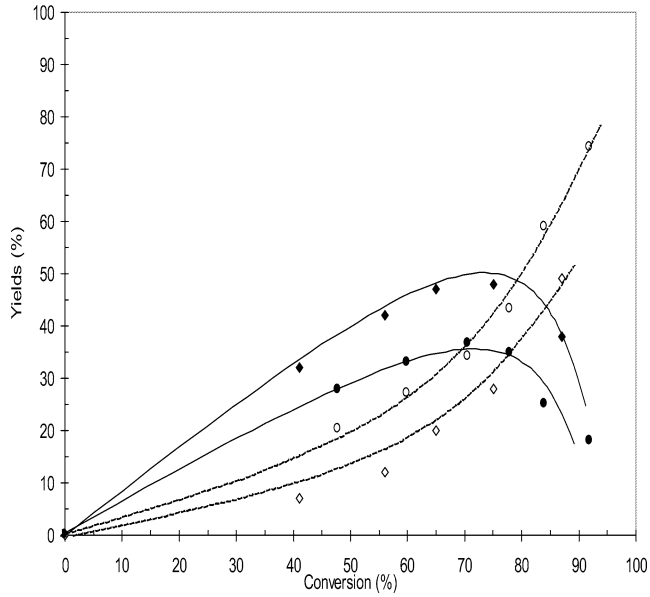

Fig. 5. C_{14} product yields (*C14prod*), (◆) at 573 K, and (●) at 603 K; and cracking yields ($C14^-$), (◇) at 573 K, and (○) at 603 K, as a function of phenanthrene conversion over the Pt/silica-alumina-1 catalyst.

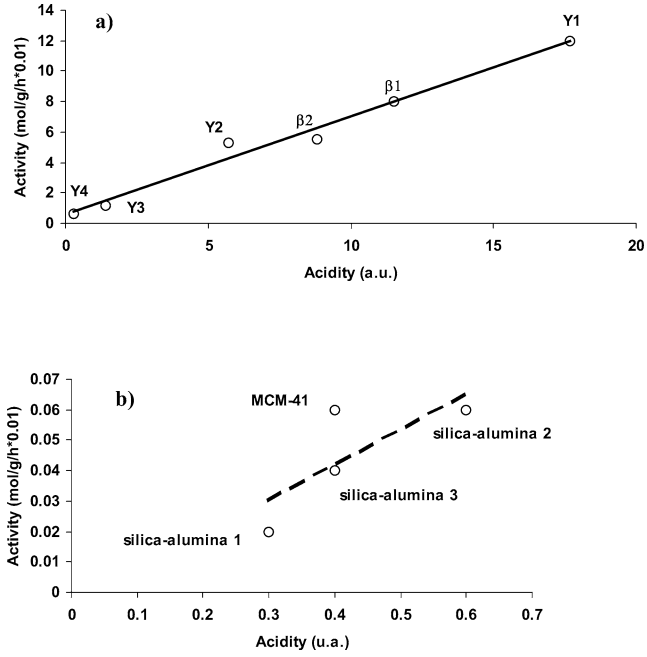

Fig. 6. Catalytic activity at $T = 573$ K in phenanthrene conversion (mol/(g h) $\times 10^{-2}$) as a function of acidity (arbitrary unit as determined by IR spectroscopy with adsorption–desorption of lutidine, see Table 3) for (a) FAU and BEA catalysts, and (b) silica-aluminas and MCM-41.

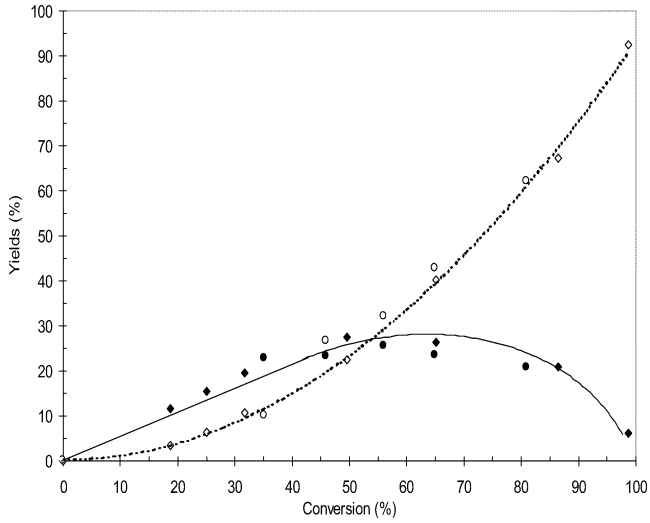

Fig. 7. C_{14} product yields (*C14prod*), (◆) over Pt/H-β1, and (●) over Pt/H-β1+NH_3; and cracking yields (*C14*$^-$), (◇) over Pt/H-β1, and (○) over Pt/H-β1+NH_3 as a function of phenanthrene conversion at $T = 573$ K.

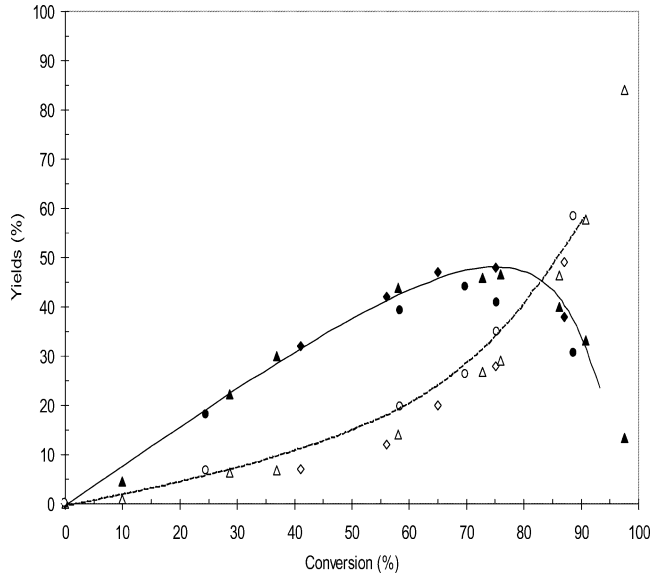

Fig. 8. C_{14} product yields (*C14prod*), (◆) over Pt/silica-alumina-1, (▲) over Pt/silica-alumina-2, (●) over Pt/silica-alumina-3; and cracking yields (*C14*$^-$), (◇) over Pt/silica-alumina-1, (△) over Pt/silica-alumina-2, and (○) over Pt/silica-alumina-3 as a function of phenanthrene conversion at $T = 573$ K.

mainly result from differences in both the number and the acid strength of acid sites. In order to investigate the effect of the acidity on selectivities, phenanthrene hydrocracking was performed on two Pt/H-β zeolites with Si/Al ratios of 10.5 and 94, corresponding to acidity indices ranging from 9.9 to 14.5 (Table 3). The textural analysis performed on these two β zeolite samples did not reveal any detectable evolution of the microporous and mesoporous volumes during the dealumination treatment. This indicates that no mesopores were created during dealumination. The two β zeolite samples showed substantial differences in activity (Fig. 6a), but not in selectivity. The absence of selectivity differences indicates that all the rate-determining steps were influenced to the same extent upon variation of the acidity of the β zeolite samples [29]. In other words, this result indicates that the rates of the isomerization and the cracking steps were modified to the same extent when the acidity of the β zeolite varied, while maintaining the structure unchanged. This result was confirmed by adding 30 wppm of aniline during the catalytic test. Aniline decomposes totally to give NH_3 and cyclohexane. The addition of NH_3 (ex-aniline), which inhibits the stronger acid sites of the β zeolite, allows a larger acidity range to be covered with indices varying from 3.0 to 14.5. These experiments showed that the activity is correlated to the acidity, whereas the isomerization and cracking yields remained unchanged for a given conversion, indicating that the selectivities are the same (Fig. 7). This is in agreement with the previous observations made on the dealuminated β zeolite sample.

The phenanthrene hydrocracking test was also performed on three Pt/silica-aluminas with different silica-content from 30 to 90 wt% (Table 2) and presenting different acidities (Table 3). The three mesoporous silica-aluminas samples showed differences in activity (Fig. 6b), but not in selectivity (Fig. 8). The Pt/MCM-41 catalyst presented the same catalytic behavior as the silica-alumina-2. As in the case of β zeolite (microporous network), the absence of selectivity differences indicates that the rates of the isomerization and the cracking steps were modified to the same extent when the acidity of the silica-alumina (mesoporous solids) varied with the silica content. Consequently from the results, it appears that for a given microporous or mesoporous structure, the acidity does not influence the selectivity into isomerization and cracking products.

In order to complete the study of the influence of acidity on selectivities, phenanthrene hydrocracking was also performed on Pt/H-Y zeolite with Si/Al of 5.7, 17.7, 38, and 73, and differences in acidity which changes in index from 0.6 to 25 as determined by IR spectroscopy with adsorption–desorption of lutidine (Table 3). The four Y zeolite samples showed substantial differences in activity correlated to the acidity (Fig. 6a), as expected. Nevertheless, contrarily to the results obtained with β zeolite and silica-alumina samples, the Y zeolite samples also presented differences in selectivities as reported in Fig. 9. Clearly the *C14prod* selectivity increases with the Si/Al ratio of the Y zeolite. The higher *C14prod* selectivity is obtained with the Y zeolite sample presenting the higher Si/Al ratio and the lower acidity (H-Y4). These results are apparently in opposition with the previous ones. However, the lutidine adsorption–desorption experiment should be considered carefully because the temperature of desorption may depend not only on the strength of the acid site but also on the dispersive forces contribution connected to pore size. This point will be discussed in the next paragraph.

Besides, we have to take into account that the Y samples with increasing Si/Al ratio are obtained by dealumi-

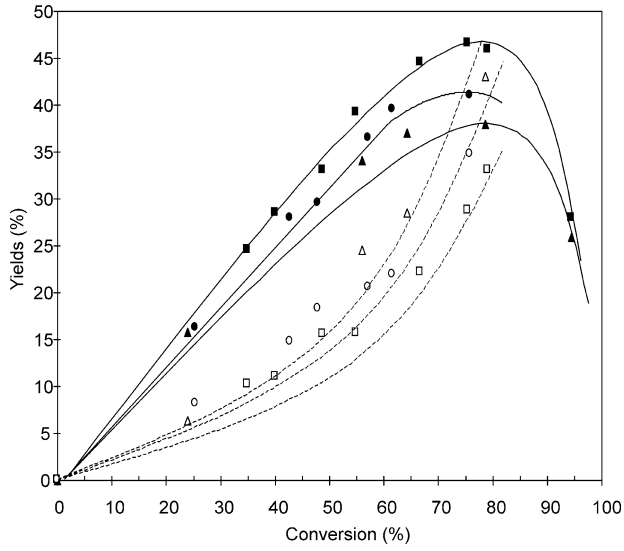

Fig. 9. C_{14} product yields (*C14prod*), (■) over Pt/H-Y4, (●) over Pt/H-Y3, (▲) over Pt/H-Y2; and cracking yields (*C14*$^-$), (□) over Pt/H-Y4, (○) over Pt/H-Y3, and (△) over Pt/H-Y2.

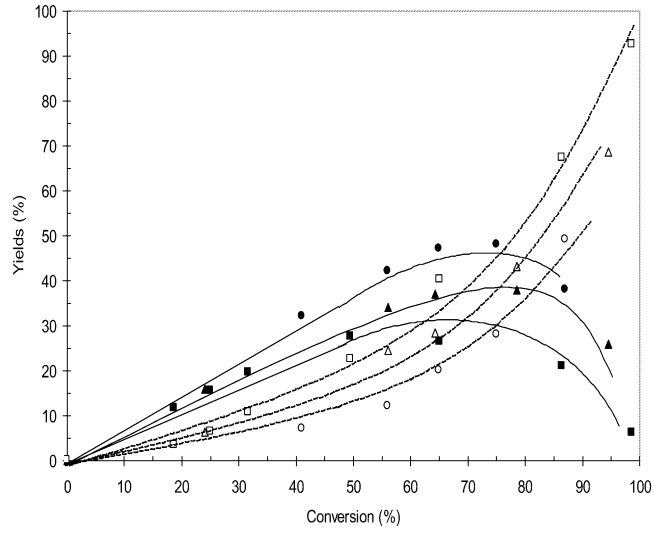

Fig. 10. C_{14} product yields (*C14prod*), (■) over Pt/H-β1, (▲) over Pt-H-Y2, (●) over Pt/silica-alumina-1; and cracking yields (*C14*$^-$), (□) over Pt/H-β1, (△) over Pt/H-Y2, and (○) over Pt/silica-alumina-1 as a function of phenanthrene conversion at 573 K.

nation treatments. These treatments lead to the formation of mesopores inside the crystals of the Y zeolite [30,31]. The stronger dealumination treatments, which allow Y zeolite samples with higher Si/Al ratios to be obtained, lead to the formation of the higher mesoporous volume as shown in Table 1. Concomitantly the size of the mesopores formed is also increased. The diameters of the mesopores varies from a range of 3–10 nm in the Y1 sample to a range of 3–60 nm in the Y4 sample, as determined by TEM. Consequently in the series of experiments concerning the Y zeolite samples, we cannot consider that the textural properties of the Y zeolite remain unchanged while the Si/Al increases.

Finally, we can conclude that the selectivity in C_{14} products (*C14prod*) and consequently in isomerization products is not controlled by the acidity in the cases of the β zeolite, MCM-41, and silica-alumina-based catalysts. However, in the case of catalysts containing Y zeolite, the simultaneous variation of two parameters (number of acid sites and textural characteristics) does not allow us to give a clear conclusion.

3.5. Effect of pore opening

In order to compare these catalysts in terms of *selectivity*, the variation of yields among the two families of products, *C14prod* and *C14*$^-$, with respect to reactant conversion was studied. The results for Pt/H-β1, Pt/H-Y2, and Pt/silica-alumina-1 catalysts are reported on Fig. 10. At 573 K, the classification obtained for *C14prod* selectivity is Pt/SiO_2-Al_2O_3(48.0%) > Pt/H-Y(38.0%) > Pt/H-β(28.5%) (in brackets is indicated the maximum yield in *C14prod*). H-β zeolite can be seen to be the most favorable structure for producing cracked products. The silica-alumina-based catalyst is the least active but exhibits the highest selectivity for the group of products including isomerized products, the *C14adam*, the bicyclohexyl, and alkylnaphtyl-type compounds, that is, products having 14 carbon atoms without loss of carbon atom compared to the reactant. When the pore aperture of the acidic solids increases, the selectivity into products with 14 carbon atoms (*C14prod*) increases simultaneously. In the case of the ZSM-5-based catalyst, the phenanthrene conversion is limited to 30% at 573 K. The *C14prod* yield is about 18%, while the cracking yield already reaches 12%. At higher temperature (603 K), the conversion can be increased up to 50%, but under these conditions the reaction products are mainly cracked products (*C14*$^-$) and products with 14 carbon atoms (*C14prod)* are hardly detectable, whereas for H-Beta catalysts, the *C14*$^-$ yields remains lower than 20% at 603 K (see Fig. 5). As we have shown in the previous paragraph that the selectivity is not governed by the acidity, such differences between crystalline and amorphous aluminosilicates should find an explanation in "structure" and pore size effects affecting either diffusion or adsorption properties.

In order to better understand these effects, we first carried out molecular simulations of the diffusion properties for three relevant products, phenanthrene, perhydrophenantrene, and methylcyclopentanodecaline inside zeolites FAU, BEA, and MFI, according to the approach described under Methods. The results reported in Table 5 indicate that phenanthrene and perhydrophenanthrene, as well as the product methylcyclopentanodecaline, exhibit no diffusion limitations in the FAU and BEA frameworks. However, it is clearly shown that for the MFI catalyst, the molecules involved in phenanthrene hydrocracking are submitted to high diffusion barriers ($\Delta E > 70$ kcal/mol). From these results, we can also assume that silica-aluminas presenting significantly larger pores than the microporous zeolites are also free of diffusion limitations. These results

Table 5
Diffusion barrier (kcal/mol) and periodicity of the diffusion pathway

Products\host structures	FAU		BEA		MFI	
	Periodicity	ΔE	Periodicity	ΔE	Periodicity	ΔE
Phenanthrene	None	14	Yes	12	Yes	70
Perhydrophenanthrene	None	20	None	30	Yes	80
Methylcyclopentanodecaline	None	25	None	11	Yes	100

might explain to some extent why the catalytic performances of MFI are rather low due to strong diffusion limitations. However, since activation energies are about the same (25–30 kcal/mol) for all catalysts including MFI based catalyst, the diffusion is not the determining step. Moreover, diffusion limitations cannot explain the selectivity differences observed among zeolite Y, β, or amorphous silica-aluminas.

Concerning the adsorption properties of molecules involved in phenanthrene hydrocracking, simulations were carried out at 573 K and with a hydrocarbon partial pressure of 100 kPa. The types of solids frameworks for this study are FAU, BEA, MFI, and VFI. Our approach cannot be applied directly to amorphous silica-aluminas due to the fact that they do not have crystallographic structures. However, in order to mimic a larger pore structure type such as found in silica-aluminas, we included the VFI zeolite, with 18 member-ring channels and a pore diameter of 12 Å, in the set of considered solids. The data collected from this work concern the adsorption energy of intermediates molecules and products involved in the phenanthrene hydrocracking, namely perhydrophenanthrene, methylcyclopentenodecaline, and methylcyclohexane. It is clear that the exact adsorption energies of olefins is made of a chemisorptive part and of a dispersive part. The contribution of the dispersive interactions is given by values in Table 6 where adsorption energies of lutidine reveal that this molecule is also submitted to the confinement effect. According to ^{1}H NMR experiments [32] carried out on FAU, MOR, and silica-aluminas, the strength of the Brønsted acid sites does not depend on the solid. As a consequence, the variation in adsorption energies should be mainly governed by the confinement effect depending on the molecular volume and pore sizes. For these reasons, we think that the temperature of lutidine desorption cannot be interpreted as a measure of the intrinsic Brønsted acid site strength but rather as a measure of number of acid sites. The results show first that for a given solid framework, the adsorption energy increases (in absolute values), when the molecular volume of the adsorbed molecule becomes larger. Simultaneously, for a given molecule (perhydrophenantrene or isomerized products), the adsorption energy (in absolute values) increases when the void space decreases:

$$\left|E^{\text{ads}}(\text{VFI})\right| < \left|E^{\text{ads}}(\text{FAU})\right| < \left|E^{\text{ads}}(\text{BEA})\right|.$$

For smaller molecular volumes (methycyclohexane and propane), the adsorption energies are the highest in MFI. These trends are consistent with the confinement effect [33–36] and will be elaborated further in a future paper. Perhydrophenantrene and methylcyclopentenodecaline are sterically excluded from the MFI framework, whereas the methylcylohexane adsorption energy is stronger in MFI than in BEA, FAU, or VFI. For propane and C_7 compound, the confinement effect leads to stronger adsorption energies in MFI than in BEA due to the smaller MFI pore sizes. As a consequence, the C_{14} conversion should take place on the external surface of the MFI crystallites. The C_7 species formed should diffuse in the MFI framework where they would be further cracked due to the stabilization of molecules with smaller molecular volume. This would explain why large amounts of cracked products (including propane and butane) are observed experimentally.

As observed similarly by Corma et al. for the *n*-heptane hydrocracking, where the iC_4 selectivity among C_4 products correlates well with the solid void spaces [37], we find that the selectivity in C_{14} products increases when the pore aperture and the void space available in the acidic solids are higher: $\beta(25\%) < \text{Y}(35\%) < \text{Si-Al}\ (45\%)$ at 60% of conversion.

In order to make a link of the products selectivities with the variation of adsorption energy of intermediary products, we define more precisely the elementary steps of the phenantrene hydroconversion in Fig. 11. It can be seen that two reaction pathways are competing: path A, leading to isomerized products; and path B, to cracked products. Since in Table 6, it is shown that for a given molecule, the adsorption energy increases when the void space decreases, this

Table 6
Adsorption energies (kcal/mol)

Reaction products	E^{ads}(MFI)	E^{ads}(BEA)	E^{ads}(FAU)	E^{ads}(VFI)
Perhydrophenanthrene	n.c.[a]	−46.4	−36.5	−29.9
Methylcyclopentanodecaline	n.c.	−47.9	−40.9	−36.5
Methylcyclohexane	−32.0	−29.8	−25.3	−23.6
Lutidine	−29.5	−24.3	−20.5	−19.0
Propane	−19.7	−14.7	−14.4	−8.6

[a] GCMC simulation results at 573 K and 100 kPa. (n.c. means that no adsorption is observed in MFI.)

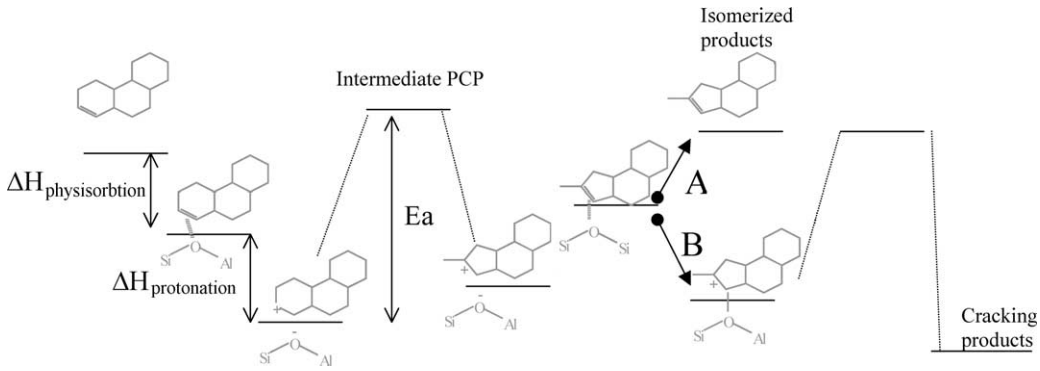

Fig. 11. Elementary steps of the phenanthrene hydrocracking highlighting the two competing pathways (A versus B) controlling the selectivity.

means that the stabilization of isomerized product is higher for solids exhibiting smaller void space. As a consequence, path A leading to the desorption and consequently to the production of isomerized products is disfavored when pore aperture is smaller. On the contrary, high adsorption energies will favor path B and the formation of the cracking products. Therefore, the selectivity in isomerized products is expected to be improved with the most opened pore structure. This is a rational explanation of our experimental observations.

In conclusion, the desorption of isomerized products is the key step allowing good selectivities into isomerization products to be obtained. The lower the adsorption energy of isomerization products, the higher the selectivity into isomerized products. This conclusion is consistent with the results presented at the end of Section 3.4 showing that the selectivity in isomerized products increased with the dealumination extent of the Y zeolite. It can reasonably be assumed that the increase of the mesopores quantity present inside Y zeolite crystals leads to a decrease of the global average adsorption energy of the intermediary and bulky products involved in the phenanthrene hydrocracking. As a consequence, this favors the desorption of isomerized products and allows higher isomerization selectivities to be reached.

4. Conclusion

The effect of the porous structure and the acidity of different acidic solids on the hydrocracking activity and selectivities was investigated via the phenanthrene hydrocracking reaction on Pt-based catalysts. Various microporous acidic solids (H-Y, H-β, and H-MFI) and mesoporous solids (amorphous silica-aluminas, and MCM-41) presenting different acid site densities were used. The acidity effect was investigated using β zeolites and silica-aluminas having different acid site densities. The results showed substantial differences in activity, which is correlated to acid site number, determined by IR spectroscopy with adsorption–desorption of lutidine but not to selectivity.

The absence of selectivity differences with acidity modifications indicates that the rates of the isomerization and cracking steps were modified to a same extent. The catalytic tests combined with molecular modeling showed that if no significant diffusional limitations are involved, the higher selectivity into isomers products is obtained with the acidic structures presenting the largest pore aperture corresponding to the lowest adsorption energy of the intermediary and bulky products involved in the hydrocracking of the phenanthrene. In the case of Y zeolite-based samples with variable Si/Al ratios, it has been shown that the observed increase in isomerization selectivity is not due to an acidity effect. In line with the analysis proposed for the other solids, an increasing amount of mesopores inside the Y zeolite crystals might contribute to the higher isomerization selectivities. However, further investigations are required to precisely identify the origin of the selectivity. The catalysts devoted to the production of middle distillate should minimize the secondary cracking reactions. Consequently the catalysts should be designed to present low adsorption energies of the desired products and, for that purpose, should exhibit an optimal confinement effect. We hope to address this optimization in a forthcoming paper.

References

[1] European Refining: The Quality Challenge, Purvin & Gertz Inc., The European Refining Technology Conference, Paris (November 22–24, 1999), 1999.
[2] P.B. Weisz, Adv. Catal. 13 (1962) 137.
[3] J. Weitkamp, Erdol Kohle Fidgas 31 (1978) 13.
[4] J. Sherzer, A.J. Gruia, Hydrocracking Science and Technology, Dekker, New York, 1996, Chap. 12.
[5] M.A. Camblor, A. Corma, A. Martinez, V. Martinez-Soria, S. Valencia, J. Catal. 179 (1998) 537.
[6] J. Ward, Fuel Process. Technol. 35 (1993) 55.
[7] A. Corma, A. Martinez, V. Martinez-Soria, J. Catal. 200 (2001) 259.
[8] J.A. Martens, P.A. Jacobs, J. Weitkamp, Appl. Catal. 20 (1986) 239.
[9] M.S. Steijns, G. Froment, P. Jacobs, J. Weitkamp, Ind. Eng. Chem. Prod. Res. Dev. 20 (1981) 654.
[10] R.F. Sullivan, J.E. Clark, G.E. Langlois, J. Catal. 3 (1964) 183.
[11] K. Sato, Y. Nishimura, H. Shimada, Catal. Lett. 60 (1999) 83.
[12] S.C. Korre, PhD thesis, University of Delaware, 1994.
[13] L. Leite, E. Benazzi, N. Marchal-George, Catal. Today 65 (2001) 214.
[14] L. Leite, E. Benazzi, N. Marchal-George, H. Toulhoat, Stud. Surf. Sci. Catal. 130 (2000) 2495.
[15] J.S. Beck, J.C. Vartulli, W.J. Roth, M.E. Leonowicz, C.T. Kersge, K.D. Schmitt, C.T.-W. Chu, D.H. Olson, E.W. Sheppard, S.B. McCullen, J.B. Higgins, J.L. Schlenker, J. Am. Chem. Soc. 114 (1992) 10834.

[16] M. Maache, A. Janin, J.C. Lavalley, J.F. Joly, E. Benazzi, Zeolites 13 (1993) 419.
[17] D. Haffad, A. Chambellan, J.C. Lavalley, Catal. Lett. 54 (1998) 227.
[18] A. Corma, C. Rodellas, V. Fornes, J. Catal. 88 (1984) 374.
[19] Sorption, Diffusion_path and UFF are distributed with Accelrys' software packages InsightII and Cerius^2 (InsightII and Cerius^2 user guides and web site: http://www.accelrys.com).
[20] A.K. Rappe, C.J. Casewit, K.S. Colwell, W.A. Goddard III, W.M. Skiff, J. Am. Chem. Soc. 114 (1992) 10024.
[21] M.P. Allen, D.J. Tildesley, Computer Simulation of Liquids, Oxford Univ. Press, Oxford, 1989.
[22] J.A. Horsley, J.D. Fellmann, E.G. Derouane, C.M. Freeman, J. Catal. 147 (1994) 231–240.
[23] N.L. Allinger, B.J. Gorden, I.J. Tyminski, J. Org. Chem. 36-6 (1971) 739.
[24] F. Alvarez, F.R. Ribeiro, G. Pérot, C. Thomazeau, M. Guisnet, J. Catal. 162 (1996) 179.
[25] L. Leite, PhD thesis, University Pierre et Marie Curie, Paris VI, 2000.
[26] A. Schneider, R.W. Warren, J. Org. Chem. 31 (1966) 1617.
[27] H.W. Haynes, AICHE Annual Meeting, New Orleans, 1981, Preprint 16B.
[28] S. Mignard, N. Marchal, Spring National Meeting of the AICHE, Atlanta, 1994, Preprint F12.
[29] J.W. Thybaut, G.B. Martin, G.V. Baron, P.A. Jacobs, J.A. Martens, J. Catal. 202 (2001) 324.
[30] Ch. Marcilly, Pet. Tech. 328 (1986) 12.
[31] A.H. Janssen, A.J. Koster, K.P. de Jong, in: Proceedings of the 13th International Zeolite Conference, Montpellier, France (July 8–13, 2001), 2001.
[32] L. Heeribout, R. Vincent, P. Batamack, C. Dorémieux-Morin, J. Fraissard, Catal. Lett. 53 (1998) 23.
[33] D. Barthomeuf, Mat. Chem. Phys. 17 (1987) 49.
[34] E.G. Derouane, J.M. André, A.A. Lucas, J. Catal. 110 (1988) 58.
[35] I. Derijcke, J.P. Vigneron, Ph. Lambin, A.A. Lucas, E.G. Derouane, J. Chem. Phys. 94 (1991) 4620.
[36] E.G. Derouane, J. Mol. Catal. A 134 (1998) 29.
[37] A. Corma, M. Davis, V. Fornes, V. Gonzalez-Alfaro, R. Lobo, J. Catal. 167 (1997) 438.